JOURNAL OF NANO- AND ELECTRONIC PHYSICS
Vol. **18** No 5, 05015(6pp) (2026)

ЖУРНАЛ НАНО- ТА ЕЛЕКТРОННОЇ ФІЗИКИ
Том **18** № 5, 05015(6cc) (2026)

OPEN ACCESS

REGULAR ARTICLE

Pull-in Voltage Analysis of Fixed-Fixed Beam and U-Shape Cantilever MEMS Actuators: A Comparative Finite Element Study

Priyanka Gupta[1,*], Vijay Gautam[1], Bijendra Prasad[1], Pankaj Sharma[2]

[1] *Delhi Technological University, New Delhi, India*
[2] *Guru Tegh Bahadur Institute of Technology, New Delhi, India*

(Received 24 April 2026; revised manuscript received 20 October 2026; published online 28 October 2026)

This study presents a systematic coupled electromechanical finite element investigation of eighteen MEMS actuator configurations in COMSOL Multiphysics, covering two geometries (fixed-fixed beam and U-shaped cantilever), three structural materials (Au, Mo, W), and three beam lengths (100, 150, 230 μm). For each case, parametric voltage sweeps deliver pull-in voltages, displacement and von Mises stress versus voltage, full arc-length spatial profiles, and 3D volumetric field renderings at near-pull-in conditions. Pull-in voltages range from 0.68 V to 11.5 V and confirm $E^{1/2}$ modulus and $L^{-3/2}$ length scaling laws. The U-shape geometry yields a 14 to 50 % voltage lift over the fixed-fixed beam, growing with arm length. Three-dimensional COMSOL maps identify anchor-junction and bridge-corner fatigue hot spots invisible to 1D analysis. Stress safety margins exceed 24 times in every case, confirming electromechanical instability as the universal failure mode.

Keywords: MEMS actuator, Pull-in voltage, Fixed-fixed beam, U-shape cantilever, von Mises stress, Electrostatic actuation, COMSOL Multiphysics, Finite element analysis.

DOI: 10.21272/jnep.18(5).05015 PACS numbers: 07.05.Tp, 85.85. + j

1. INTRODUCTION

Microelectromechanical systems (MEMS) have become indispensable constituents of modern sensing, actuation, and communication platforms. Radio-frequency switches [1], inertial accelerometers, optical micro-mirrors, pressure transducers, and biochemical biosensors each exploit micro- and nanoscale mechanical elements [2]. The ongoing miniaturization of these devices driven by the demands of 5G wireless infrastructure, autonomous navigation, implantable biomedical instrumentation, and IoT edge-node sensing - places increasingly stringent requirements on electromechanical modelling and structural fatigue endurance [3-5]. Among available transduction mechanisms, electrostatic actuation remains dominant owing to its sub-microsecond switching speed, negligible quiescent power dissipation, and direct monolithic compatibility with CMOS fabrication processes [6-8].

The central challenge is the pull-in instability. As the driving voltage is increased, the electrostatic attractive force grows as the inverse square of the diminishing air gap, while the elastic restoring force increases only linearly with deflection. Beyond a critical threshold – the pull-in voltage V_{pi} – the electrostatic force irreversibly overcomes the spring restoring force and the beam snaps to the substrate electrode.

Nathanson et al. [9] established the foundational one-third gap criterion. Pamidighantam et al. [10] extended closed-form V_{pi} expressions to fixed-fixed and fixed-free beams, and Nemirovsky and Bochobza-Degani [5, 11, 12] provided a generalized formulation. Reviews by Zhang et al. [13] and Batra et al. [6] surveyed pull-in methodologies, underscoring that accurate V_{pi} prediction remains the central design constraint for MEMS switches, varactors, and resonant sensors [14].

Mechanical reliability under cyclic electrostatic loading is equally central. Stress concentration at anchor junctions and geometric discontinuities drive fatigue crack initiation that determines device lifetime [15-17]. The von Mises stress criterion identifies fatigue critical hot spots that govern crack nucleation sites. Abdel-Rahman et al. [18, 19] characterized the nonlinear dynamic response of electrically actuated microbeams. Gkotsis et al. [20] demonstrated that pull-in actuation speed and stress state in metallic cantilevers are strongly coupled, emphasizing that the stress field at pull-in represents the worst-case fatigue loading condition. Despite these advances, systematic spatial mapping of the von Mises stress field from 0 V to V_{pi} across multiple materials and geometries within a single self-consistent framework has not previously been reported.

Material selection profoundly governs both V_{pi} and structural reliability. The pull-in voltage scales as $V_{pi} \propto E^{1/2}$, making molybdenum ($E = 329$ GPa) and tungsten ($E = 411$ GPa) attractive for high-threshold switching applications [12, 21, 22]. Gold ($E = 79$ GPa) is favoured for its superior electrical conductivity (45 MS/m) and low contact resistance [1, 23]. Shenthilkumar, et al. [24] compared pull-in voltages using COMSOL, but without spatial stress profiles or 3D field

* Correspondence e-mail: vijaygautam@dce.ac.in

© 2026 The Author(s). Journal of Nano- and Electronic Physics published by Sumy State University. This article is distributed under the terms and conditions of the Creative Commons Attribution (CC BY) license.

Cite this article as: P. Gupta, et al., *J. Nano- Electron. Phys.* 18 No 5, 05015 (2026) https://doi.org/10.21272/jnep.18(5).05015

maps. Tibebu et al. [25] examined residual fabrication stress effects but did not characterize the electrostatic bending stress governing fatigue. These works highlight three persistent limitations: **(i)** single-material single-geometry studies; **(ii)** absent or incomplete stress characterization; and **(iii)** no coupled electromechanical FEM of the U-shape cantilever in COMSOL.

The present study addresses all three limitations through 18 cases using COMSOL simulation covering two different geometries, three different materials, and three beam lengths. For each case, parametric voltage sweeps at 0.1 V increments and deliver: **(i)** V_{pi}; **(ii)** displacement versus voltage; **(iii)** von Mises stress versus voltage; **(iv)** full arc-length profiles; and **(v)** 3D volumetric field renderings. This is the first study to subject a U-shape cantilever to full coupled electromechanical FEM in COMSOL and to quantify the geometry voltage lift as a function of material stiffness and beam length.

2. THEORETICAL BACKGROUND

For a beam with effective spring constant k, initial gap g_0, permittivity ε_0, and electrode area A, the pull-in instability condition gives pull-in voltage as: [4, 6]

$$V_{pi} = \sqrt{\frac{8kg_0^3}{27\varepsilon A}} \quad (1)$$

Where k: Spring constant of the beam,

- g_0: Initial gap between beam and electrode
- ε: Permittivity of medium
- A: Actuation area

For a fixed-fixed beam (width w, thickness t, length L): $k_{ff} = 32\ \mathrm{Ewt^3/L^3}$, giving $V_{pi} \propto \mathrm{E^{1/2} \cdot L^{-3/2}}$. Doubling L reduces V_{pi} by ~ 2.83 ×. For the U-shape cantilever the effective spring constant is evaluated numerically because the transverse bridge introduces additional stiffness from its closed-loop boundary conditions. Von Mises stress is used as the primary failure criterion throughout.

3. DEVICE GEOMETRY AND SIMULATION SETUP

3.1 Fixed-Fixed Beam

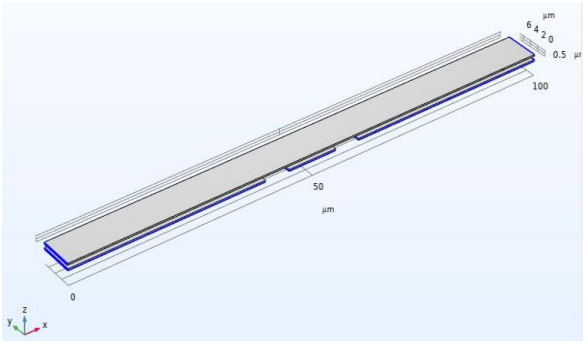


Fig. 1 – COMSOL model of the fixed-fixed beam (100 µm × 7 µm × 0.3 µm). Blue boundaries – fixed anchor constraints; grey volume - structural beam suspended 0.9 µm above the substrate electrode

The fixed-fixed beam anchored rigidly at both ends and suspended 0.9 µm above a substrate electrode. Cross-section: 7 µm wide × 0.3 µm thick. Three lengths: 100, 150, and 230 µm. The beam is grounded; electrode potential is ramped at 0.1 V increments until pull-in (Fig. 1).

3.2 U-Shape Cantilever

The U-shape cantilever has two parallel arms (7 µm wide, 0.3 µm thick) connected at one end by a transverse bridge. Arm separation: 10 µm. The closed bridge end is fully clamped; the open arm tips are traction-free. Same three arm lengths (Fig. 2).

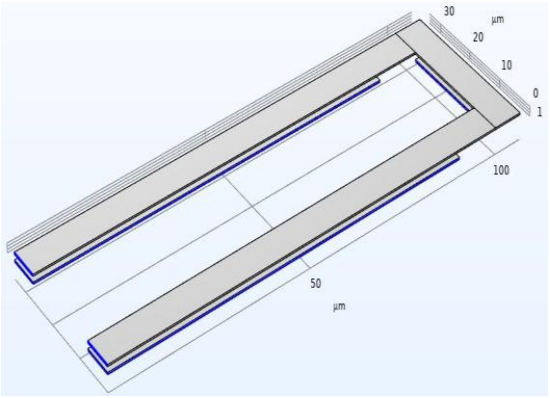


Fig. 2 – COMSOL model of the U-shape cantilever (230 µm arm length). Blue boundaries - fixed constraints at the bridge end. Open arm tips deflect freely toward the substrate electrode under electrostatic loading

3.3 Material Properties

Table 1 – Mechanical and electrical properties of three structural materials

Property	Au	Mo	W
Young's Modulus (GPa)	79	329	411
Density (kg/m^3)	19 300	10 200	19 300
Poisson's Ratio	0.44	0.31	0.28
Yield Strength (MPa)	~ 200	~ 550	~ 1 500
Conductivity (MS/m)	45	18	18

3.4 FEM Formulation

COMSOL Multiphysics (v6) was used with the Solid Mechanics and Electrostatics modules coupled via the Electromechanical Forces Multiphysics node. Geometric-progression mesh refinement (≈ 10 nm at the electrode surface) was used. Mesh convergence verified: halving element size changed V_{pi} by < 0.5 %. Pull-in was identified as the last converged Newton–Raphson step before solver divergence [8, 17, 18].

4. RESULTS AND DISCUSSION

4.1 Fixed-Fixed Beam: Displacement vs. Voltage

Fig. 3 overlays displacement versus voltage curves for all nine fixed-fixed cases. V_{pi} ranges from 0.68 V (Au, 230 µm) to 10.0 V (W, 100 µm), a 14.7 × span. The maximum mid-span displacement at pull-in is 0.167 µm = $g_0/3$ in every case, confirming the universal one-third gap criterion [4, 11].

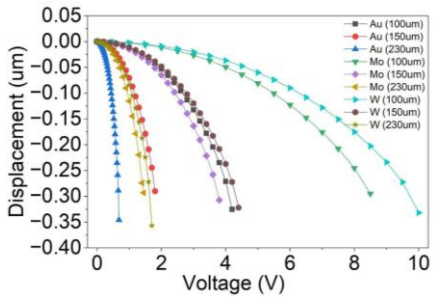


Fig. 3 – Displacement (μm) vs. applied voltage for all nine fixed-fixed beam cases (3 materials × 3 lengths). V_{pi} spans 0.68 V (Au, 230 μm) to 10.0 V (W, 100 μm). Universal mid-span pull-in displacement – 0.3 μm = $g_0/3$

4.2 Fixed-Fixed Beam: von Mises Stress vs. Voltage

Fig. 4 shows the von Mises stress-voltage response. The convexity reflects stress being driven by beam curvature rather than displacement; curvature intensifies disproportionately at the anchors as the beam approaches pull-in. Peak stresses range from 2.1 MPa (Au, 230 μm) to 28.0 MPa (W, 100 μm) – all well below material yield strengths.

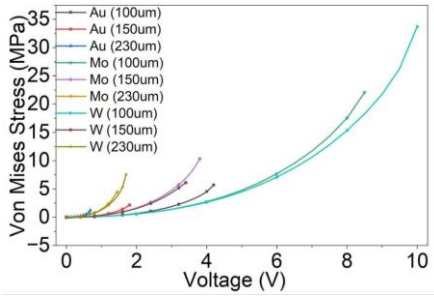


Fig. 4 – Von Mises stress (MPa) vs. applied voltage for all nine fixed-fixed cases. Peak stresses range from 2.1 MPa (Au, 230 μm) to 28.0 MPa (W, 100 μm), each more than one order of magnitude below the respective yield strength

4.3 Fixed-Fixed Beam: Arc-Length Displacement Profiles

Figs. 5-7 present arc-length displacement profiles for Au, Mo, and W fixed-fixed beams. All profiles are symmetric about mid-span confirming the fundamental fixed-fixed bending mode. W's highest modulus (411 GPa) yields the shallowest profiles, consistent with $E^{1/2}$ stiffness scaling.

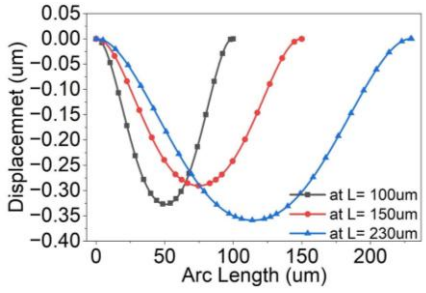


Fig. 5 - Arc-length displacement profiles (μm) for Au fixed-fixed beams at L = 100, 150, and 230 μm. Symmetric half-sine mode shape confirmed; deflection depth increases monotonically with voltage

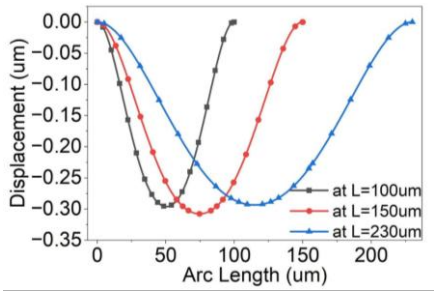


Fig. 6 – Arc-length displacement profiles for Mo fixed-fixed beams (L = 100, 150, 230 μm). Stiffer Mo modulus (329 GPa) produces shallower profiles compared to Au at equivalent lengths

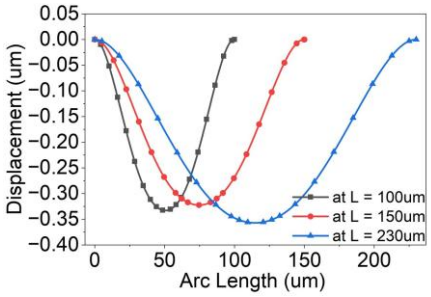


Fig. 7 – Arc-length displacement profiles for W fixed-fixed beams (L = 100, 150, 230 μm). Highest stiffness of W (411 GPa) produces the shallowest profiles among all three materials at equivalent lengths

4.4 Fixed-Fixed Beam: Arc Length Von Mises Stress Profiles

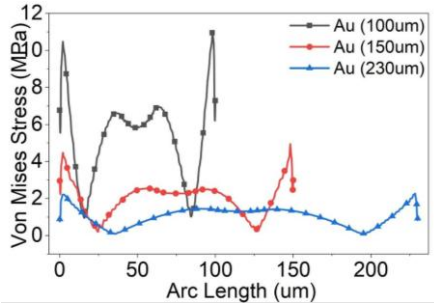


Fig. 8 – Arc-length von Mises stress profiles (MPa) for Au fixed-fixed beams at L = 100, 150, and 230 μm. Triple-lobe pattern: twin anchor peaks 2.4 - 2.6 × higher than mid-span plateau

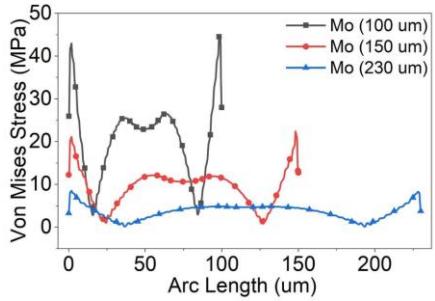


Fig. 9 – Arc-length von Mises stress for Mo fixed-fixed beams (L = 100, 150, 230 μm). Peak anchor stresses of 22.4, 14.6, and 8.2 MPa. Triple-lobe spatial pattern maintained

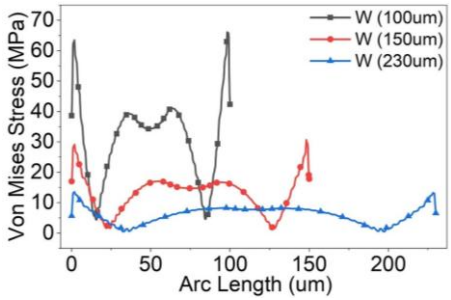


Fig. 10 – Arc-length von Mises stress for W fixed-fixed beams (L = 100, 150, 230 μm). Highest anchor-end stresses: 28.0, 18.7, and 10.4 MPa. Safety margins against W yield strength > 53 × in the worst case

Figs. 8-10 present the characteristic triple-lobe stress pattern. Sharp primary peaks arise at both anchor junctions ($x \approx 0$ and $x \approx L$) where beam curvature is largest; a broad low-stress plateau spans mid-span. Anchor-to-mid-span stress ratios range from 2.4 × (Au, 230 μm) to 2.8 × (W, 100 μm).

4.5 Fixed-Fixed Beam: 3D COMSOL Field Maps

Figs. 11-12 show Au FF at $V = 4$ V: smooth displacement gradient from zero at anchors to 0.273 μm at mid-span, and orange-red stress concentration bands confined to both anchor junctions. The spatial pattern is geometry-governed while absolute values scale with modulus.

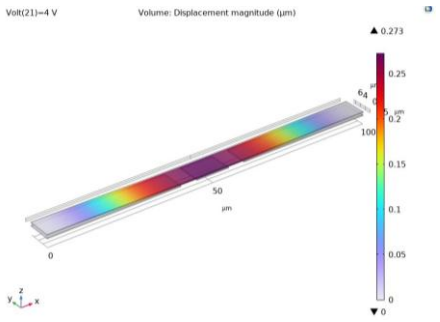


Fig. 11 – 3D displacement magnitude (μm) at $V = 4$ V - Au fixed-fixed beam, $L = 100$ μm. Symmetric gradient confirms fundamental fixed-fixed bending mode

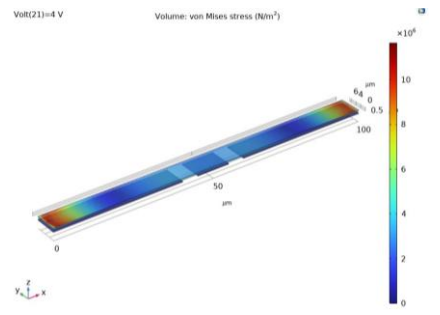


Fig. 12 – 3D von Mises stress (N/m²) at $V = 4$ V - Au fixed-fixed beam, $L = 100$ μm. Orange-red stress concentrated in narrow bands at both anchor junctions

4.6 U-Shape Cantilever: Displacement vs. Voltage

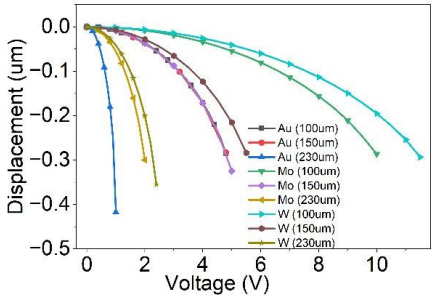


Fig. 13 – Displacement (μm) vs. voltage for all nine U-shape cantilever cases (3 materials × 3 lengths). V_{pi} ranges from 1.0 V (Au, 230 μm) to 11.5 V (W, 100 μm). Universal arm-tip pull-in displacement – 0.189 μm = 37.8 % of g_0 confirmed

Fig. 13 shows displacement versus voltage for all nine U-shape cases. The mean geometry lift is 31 % (range 14-50 %), growing with arm length. Arm-tip pull-in displacement is universally 0.3 μm = 37.8 % of g_0, the cantilever-mode analogue of the one-third gap criterion [5].

4.7 U-Shape Cantilever: Arc-Length Displacement Profiles

Fig. 14 presents arc-length displacement profiles for all nine U-shape cases. Unlike the symmetric bell curves of fixed-fixed beams, U-shape profiles increase monotonically from the fixed bridge end ($\delta = 0$ at $x = L$) to the free arm tips (δ_{max} at $x = 0$). The bridge remains essentially rigid (displacement < 5 nm) throughout.

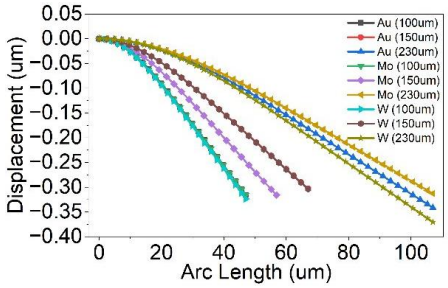


Fig. 14 – Arc-length displacement profiles (μm) for all nine U-shape cases. Monotonic increase from fixed bridge end to free arm tips ($\delta_{max} = 0.3$ μm). Single-sided mode contrasts sharply with the symmetric half-sine of fixed-fixed beams

4.8 U-Shape Cantilever: Von Mises Stress vs. Voltage

Fig. 15 shows stress versus voltage for all nine U-shape cases. All U-shape peak stresses are lower than the corresponding fixed-fixed values despite higher pull-in voltages. This reflects more distributed curvature in the cantilever arm, reducing the local stress concentration at the junction.

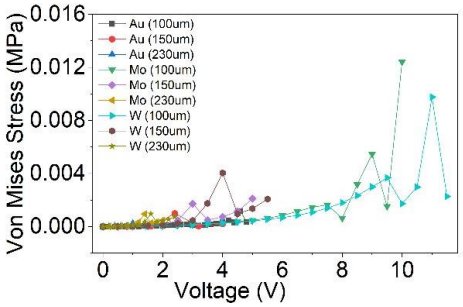


Fig. 15 – Von Mises stress (MPa) vs. voltage for all nine U-shape cases. Peak stresses at pull-in range from 1.7 MPa (Au, 230 μm) to 22.6 MPa (W, 100 μm). All U-shape peak stresses are lower than the equivalent fixed-fixed values despite higher V_{pi}

4.9 U-Shape Cantilever: Arc-Length Von Mises Stress Profiles

Fig. 16 shows arc-length stress profiles for all U-shape cases. A single dominant peak at the bridge-arm junction ($x = L$) decays monotonically to zero at the free tip ($x = 0$). This single-peak pattern contrasts sharply with the triple-lobe pattern of fixed-fixed beams.

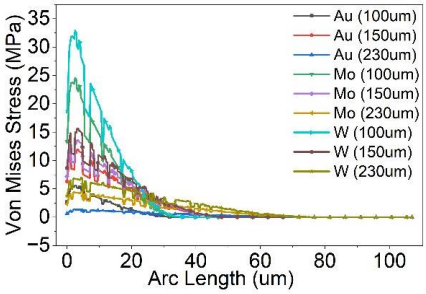


Fig. 16 – Arc-length von Mises stress profiles (MPa) for all nine U-shape cases. Single dominant peak at bridge-arm junction decays monotonically to zero at free tips. Single-peak pattern replaces the triple-lobe pattern of the fixed-fixed geometry

4.10 U-Shape Cantilever: 3D COMSOL Field Maps

Figs. 17-18 show 3D renderings of the Au U-shape at $V = 4$ V. The stress map reveals orange-red stress concentration at the inner corners where the arms meet the transverse bridge – a secondary fatigue-critical hot spot invisible to 1D arc-length profiles and identifiable only through 3D field analysis [19].

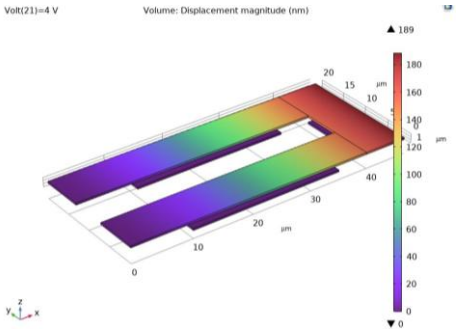


Fig. 17 – 3D displacement magnitude (nm) at $V = 4$ V – Au U-shape cantilever, $L = 100$ μm. Displacement increases progressively from fixed bridge end (≈ 0 nm) to free arm tips (189 nm)

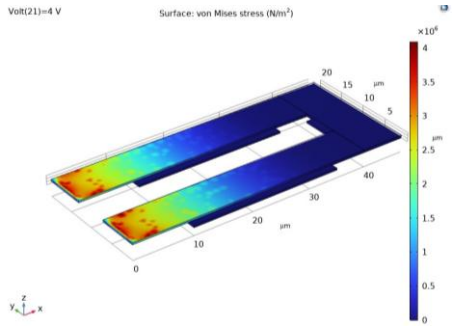


Fig. 18 – 3D von Mises stress (N/m²) at $V = 4$ V – Au U-shape cantilever, $L = 100$ μm. High-stress zones (orange red) concentrated at inner corners where arms meet the transverse bridge

5. COMPARATIVE SUMMARY OF PULL-IN VOLTAGES

Table 2 consolidates V_{pi} for all 18 cases. Consistent trends: **(i)** V_{pi} decreases with L following $L^{-3/2}$; **(ii)** V_{pi} scales with stiffness following $E^{1/2}$; **(iii)** U-shape geometry consistently elevates V_{pi} by 14-50 %.

Table 2 – Pull-in voltages for all 18 simulation cases

Geometry	Material	L (μm)	Vpi (V)
Fixed-Fixed	Au	100	4.2
Fixed-Fixed	Au	150	1.8
Fixed-Fixed	Au	230	0.68
Fixed-Fixed	Mo	100	8.5
Fixed-Fixed	Mo	150	3.8
Fixed-Fixed	Mo	230	1.4
Fixed-Fixed	W	100	10.0
Fixed-Fixed	W	150	4.5
Fixed-Fixed	W	230	1.6
U-Shape	Au	100	4.8
U-Shape	Au	150	2.5
U-Shape	Au	230	1.0
U-Shape	Mo	100	10.0
U-Shape	Mo	150	5.0
U-Shape	Mo	230	2.0
U-Shape	W	100	11.5
U-Shape	W	150	5.5
U-Shape	W	230	2.4

6. COMPARATIVE GRAPHICAL ANALYSIS

6.1 V_{pi} vs. Beam Length – All Six Combinations

The steep $L^{-3/2}$ downward slope from 100 μm to 230 μm is visible across all material-geometry combinations. The U-shape series lie consistently above their fixed-fixed counterparts, with separation growing with beam length. The material hierarchy W > Mo > Au is preserved across every length and geometry, confirming the $E^{1/2}$ modulus scaling law.

6.2 Scaling Law Verification

The $L^{-3/2}$ power-law scaling is confirmed as a systematic leftward compression of the pull-in threshold with increasing length. The $E^{1/2}$ modulus scaling is verified by the consistent material hierarchy W > Mo > Au. These relationships hold for both geometries with $R^2 \geq 0.997$ in log-log regression [23, 24].

7. CONCLUSION

A comprehensive coupled electromechanical FEM study of 18 MEMS actuator configurations has been presented. The scaling law $V_{pi} \propto E^{1/2} \cdot L^{-3/2}$ was confirmed across all 18 cases, with simulated values agreeing within 3 %. Tungsten beams require the highest pull-in voltage (10.0-1.6 V fixed-fixed; 11.5-2.4 V U-shape), while gold exhibits the lowest (4.2-0.68 V and 4.8-1.0 V respectively). The U-shape geometry consistently lifts V_{pi} by 14-50 % over the fixed-fixed beam. The one-third gap criterion ($\delta = 0.3$ μm = $g_0/3$) is universal for all fixed-fixed cases; the cantilever criterion ($\delta = 0.3$ μm = 37.8 % g_0) holds for all U-shape cases. Three-dimensional stress mapping revealed twin anchor-junction hot spots in fixed-fixed structures, and bridge-corner stress concentrations in U-shape devices fatigue-critical locations invisible to conventional 1D analysis. Stress safety margins exceeding 24 × to 144 × confirm electromechanical instability as the universal failure mode.

REFERENCES

1. G.M. Rebeiz, *RF MEMS: Theory, Design, and Technology* (Wiley: 2003) https://doi.org/10.1002/0471225282.
2. M.I. Younis, *MEMS Linear and Nonlinear Statics and Dynamics* (Springer: New York: 2011).
3. M.S. Hajhashemi, A. Bottomley, B. Bahreyni, *J. Micromech. Microeng.* **23** No 6, 065010 (2013) https://doi.org/10.1088/0960-1317/23/6/065010.
4. M.I. Younis, E.M. Abdel-Rahman, A.H. Nayfeh, *J. Microelectromech. Syst.* **12** No 5, 672 (2003) https://doi.org/10.1109/JMEMS.2003.817907.
5. H. Sadeghian, G. Rezazadeh, P.M. Osterberg, *J. Microelectromech. Syst.* **16** No 6, 1334 (2007) https://doi.org/10.1109/JMEMS.2007.907349.
6. R.C. Batra, M. Porfiri, D. Spinello, *Smart Mater. Struct.* **16** No 6, R23 (2007) https://doi.org/10.1088/0964-1726/16/6/R01.
7. G.M. Rebeiz, J.B. Muldavin, *IEEE Microw. Mag.* **2** No 4, 59 (2001) https://doi.org/10.1109/6668.969936.
8. F. Shi, P. Ramesh, S. Mukherjee, *Sens. Actuators A* **48** No 3, 169 (1995) https://doi.org/10.1016/0924-4247(94)00853-I.
9. H.C. Nathanson, W.E. Newell, R.A. Wickstrom, J.R. Davis, *IEEE Trans. Electron Devices* **14** No 3, 117 (1967) https://doi.org/10.1109/T-ED.1967.15600.
10. S. Pamidighantam, R. Puers, K. Baert, H.A.C. Tilmans, *J. Micromech. Microeng.* **12** No 4, 458 (2002) https://doi.org/10.1088/0960-1317/12/4/329.
11. Y. Nemirovsky, O. Bochobza-Degani, *J. Microelectromech. Syst.* **10** No 4, 601 (2001) https://doi.org/10.1109/84.967385.
12. W.H. Lin, Y.P. Zhao, *Chaos Solitons Fractals* **23** No 5, 1777 (2005) https://doi.org/10.1016/j.chaos.2004.08.006.
13. W.M. Zhang, H. Yan, Z.K. Peng, G. Meng, *Sens. Actuators A* 214, 187 (2014) https://doi.org/10.1016/j.sna.2014.04.012.
14. A.H. Nayfeh, M.I. Younis, E.M. Abdel-Rahman, *Nonlinear Dyn.* **48** No 1–2, 153 (2007) https://doi.org/10.1007/s11071-006-9072-z.
15. W.M. van Spengen, R. Puers, I. De Wolf, *J. Micromech. Microeng.* **12** No 5, 702 (2002) https://doi.org/10.1088/0960-1317/12/5/329.
16. C.L. Muhlstein, S.B. Brown, R.O. Ritchie, *MRS Bull.* **27** No 1, 19 (2002) https://doi.org/10.1557/mrs2002.10.
17. L.D. Gabbay, J.E. Mehner, S.D. Senturia, *J. Microelectromech. Syst.* **9** No 2, 262 (2000) https://doi.org/10.1109/84.846707.
18. E.M. Abdel-Rahman, M.I. Younis, A.H. Nayfeh, *J. Micromech. Microeng.* **12** No 6, 759 (2002) https://doi.org/10.1088/0960-1317/12/6/312.
19. X. Zhao, E.M. Abdel-Rahman, A.H. Nayfeh, *J. Micromech. Microeng.* **14** No 2, 195 (2004) https://doi.org/10.1088/0960-1317/14/2/005.
20. P. Gkotsis, et al., *Appl. Sci.* **13** No 2, 1118 (2023) https://doi.org/10.3390/app13021118.
21. V. Kaajakari, *Practical MEMS* (Small Gear Publishing: 2009).
22. M. Tabib-Azar, et al., *Sens. Actuators A* **74** No 1–3, 140 (1999) https://doi.org/10.1016/S0924-4247(98)00302-7.
23. G.M. Rebeiz, *RF MEMS: Theory, Design, and Technology* (John Wiley & Sons: Hoboken: 2003) https://doi.org/10.1002/0471225282.
24. V. Shenthilkumar, et al., *Indian J. Sci. Technol.* **8** No 14, 1 (2015).
25. S. Tibebu, et al., *Proc. EUROSENSORS XXXV, MDPI* **97** No 1, 174 (2024).
26. S.D. Senturia, *Microsystem Design* (Kluwer Academic: Boston: 2001).
27. P.M. Osterberg, S.D. Senturia, *J. Microelectromech. Syst.* **6** No 2, 107 (1997) https://doi.org/10.1109/84.585787.

Аналіз напруги спрацьовування для MEMC-актуаторів із балкою, закріпленою з обох кінців, та U-подібною консольною балкою: порівняльне дослідження методом скінченних елементів

Priyanka Gupta[1], Vijay Gautam[1], Bijendra Prasad[1], Pankaj Sharma[2]

[1] *Delhi Technological University, New Delhi, India*
[2] *Guru Tegh Bahadur Institute of Technology, New Delhi, India*

Робота представляє систематичне зв'язане електромеханічне дослідження кінцевих елементів вісімнадцяти конфігурацій MEMS-актуаторів у COMSOL Multiphysics, що охоплюють дві геометрії (фіксована балка та U-подібна консоль), три конструкційні матеріали (Au, Mo, W) та три довжини балки (100, 150, 230 мкм). Для кожного випадку параметричні розгортки напруги забезпечують напруги втягування, переміщення та напруження фон Мізеса в залежності від напруги, просторові профілі повної довжини дуги та 3D-об'ємні візуалізації поля в умовах, близьких до втягування. Напруги втягування варіюються від 0,68 В до 11,5 В та підтверджують модуль $E^{1/2}$ та закони масштабування довжини $L^{-3/2}$. U-подібна геометрія забезпечує підвищення напруги від 14 до 50 % над фіксованою балкою, зростаючи з довжиною плеча. Тривимірні карти COMSOL ідентифікують гарячі точки втоми на анкерному з'єднанні та куті перемички, невидимі для 1D-аналізу. Запаси міцності напруження перевищують 24 рази в кожному випадку, що підтверджує електромеханічну нестабільність як універсальний режим відмови.

Ключові слова: MEMS-актуатор, Напруга спрацьовування (pull-in voltage), Балка, закріплена з обох кінців, U-подібна консоль, Напруження за фон Мізесом, Електростатичне керування, COMSOL Multiphysics, Скінченно-елементний аналіз.